Journal of Rajasthan Academy of Physical Sciences
ISSN: 0972-6306; URL: http://raops.org.in
Vol.21, No.1&2, January-June, 2022, 83-100

IRREVERSIBILITY ANALYSIS FOR NON NEWTONIAN FLUIDICS INSIDE A CHANNEL: DIFFERENTIAL TRANSFORM METHOD

Paresh Vyas, Manvi Adha and Gajanand
Department of Mathematics
University of Rajasthan, Jaipur - 302004
E-mail: pvyasmaths@gmail.com, manvi.maths11@gmail.com, cv94hj@gmail.com

Abstract. The paper offers differential transform method strategy to compute entropy for Couette non-Newtonian MHD fluid flow. The flow takes place in a horizontally placed channel composed of upper impermeable wall and naturally permeable bottom. The motion sets in by the movement of upper wall that bears uniform velocity. The lower wall of the channel is a natural porous bed that enables hydrodynamic slip. Since there is no external pressure gradient, therefore the filter velocity in the porous region is assumed to be zero. This assumption is valid as per Saffman condition. The channel walls bear different uniform temperatures. The phenomenon constitutes a non-linear boundary value problem for which differential transform method is invoked to get velocity and temperature distributions in power series. The DTM solution has been compared with numerical solution derived by Runge Kutta Fehlberg 45 strategy. A rigorously computed data set for the Skin friction and Nusselt number has also been presented. The findings showcased in tables and graphs are discussed.

Key words: Non-Newtonian fluid, Channel, Entropy, Porous media.

1. Introduction

Thermo-fluidics pertaining to non-Newtonian fluids is central to numerous industrial and technological know-how such as hot rolling, lubrication, cooling problems, drag reduction, bioengineering, metallurgy, cosmetics, polymers to name a few. The importance of the domain stems from the reason that variety of fluids of interest are essentially non Newtonian. Mathematical treatment to non-Newtonian fluidics is cumbersome as contrary to Newtonian behaviour, non-Newtonian fluids show non-linear strain stress relation. It results into more non linearity in already non-linear Navier-Stokes equation. Mathematical treatment to highly non-linear system is always a daunting task. Vast literature is available on non-Newtonian fluidics with varied solution strategies in different flow geometries in clear and porous medium. One of the foremost among these is in channels as they constitute rather simpler but core source of information. Besides numerical endeavours, attempts have been made to find exact /analytical/semi analytical

solutions though such solutions are possible for basic flows in simple geometries only. Griffiths [10] derived exact solutions for shear-thinning and shear-thickening. He considered pressure-driven flow wherein viscosity followed Carreau equation. He developed requirements for existence of such analytical solutions. Raisi et al. [18] investigated Couette-Poiseuille flow of the Giesekus fluid and developed an approximate solution. Ravanchi et al. [19] reported Giesekus viscoelastic fluid flow in an annulus. Alves et al. [1] treated steady Phan-Thien-Tanner fluid flow in pipe and channel. Oliveira and Pinho [17] reported analytical solution for fully developed Phan-Thien-Tanner fluids flow in channel and pipe. Azaiez et al.[2] considered visco-elastic flows in a planar contraction and treated the model numerically. Schleiniger and Weinacht [22] treated steady Giesekus Poiseuille flow. Yoo and Choi [35] considered one-mode Giesekus shear flow. Ferrás et al. [9] derived analytical solutions for Phan-Thien-Tanner and Giesekus fluidics inside channels experiencing slip. Mitsoulis and Hatzikiriakos [16] studied slip boundary condition' impact on polymer extrusion. Chen and Zhu [7] considered slip effects on Bingham Couette-Pouisieille flow. Besides flow and heat transfer aspects, entropy in thermodynamic performance is a pertinent issue for cost effectiveness. It relies on the efficient exploitation of energy and optimal consumption of resources. Needless to say that optimal thermodynamic efficiency stands for the case when there is minimum entropy generation. It has been realized that a theoretical treatment to thermofluidics can be undertaken for thermodynamic efficiency based on second law. Bejan[4-5] shown that thermo-fluidic systems are essentially irreversible where entropy can be simulated by invoking second law of thermodynamics. Since then the domain has received much attention. Mahmud and Fraser [15] examined channel flows of non-Newtonian fluids for entropy aspects. Yilbas et al. [34] examined the problem for constant viscosity case in annular pipe. Hosseini et al. [11] considered non-Newtonian fluid flow inside a porous channel in an axisymmetric setup. Ibanez et al. [13] devised optimum slip flow by minimizing entropy generation in microchannels. Ibanez et al. [12] investigated entropy in microchannel under the influence of hydrodynamic slip and uniform heat flux. Lopez de haro et al. [14] investigated entropy in channel flow of power-law fluid. Vyas and srivastava [26] presented an analytical study of entropy arising inside a composite duct. Vyas and Soni [31] considered partial slip effect on radiating flow past a melting surface with. Vyas and Ranjan [32] presented a unique entropy generation study for meek temperature dependent convection mechanism. Bataineh et al. [3] invoked Bernstein method for second grade fluid channel flow. Devkar et al. [8] examined a straight uniform square duct facilitating fully developed non-Newtonian flow. Rosales et al. [20] studied MHD couple stress nanofluidics inside inclined channel for entropy aspects. Vyas et al. [30] employed DTM and R-K Fehlberg 45solution strategy to simulate entropy generated in couple stress Micropolar flow in Forchheimer channel. Vyas et al. [28] conducted a study with Cattaneo-Christov heat flux criterion for Casson flow inside a cone in order to get a picture of associated inherent irreversibility. Vyas and Yadav [23] exploited Keller Box scheme for examining induced magnetic field effects on entropy in time dependent free convection in a channel. Vyas et al. [29] considered Cattaneo-Christov flux to conduct a parametric study for entropy in fluidics past a shrinking sheet.

In this paper, we study thermodynamic irreversibility encountered by a non-Newtonian MHD fluid flow facilitated inside a channel. The chief objectives of the study are two fold. Firstly, to explore the possibility of applying semi analytical Differential Transform Method and its validation by a competent numerical method. Secondly, to have a parametric study of entropy generation. It is expected that the study would help amplify many industrial and thermal engineering processes involving where minimizing entropy generation might be crucial to devise optimal system. In this backdrop, the present study is a pertinent test model for future larger complex systems.

Mathematical Model

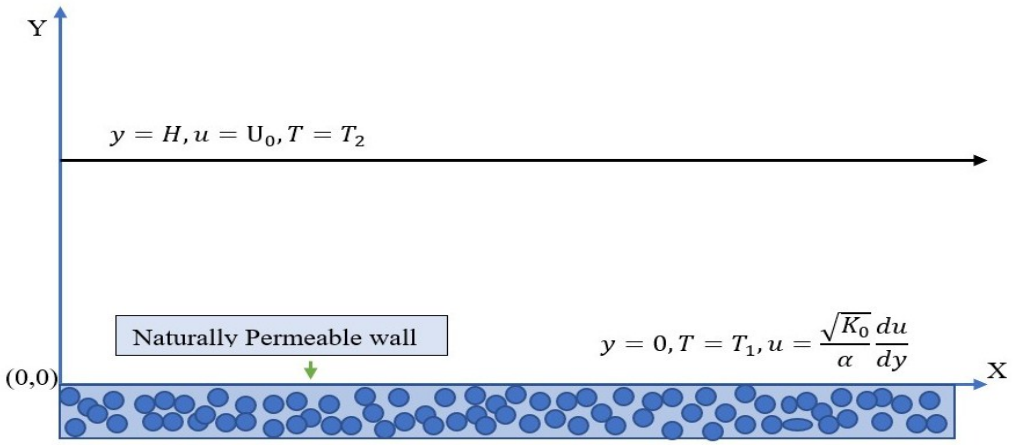

Figure-1

Consider a steady flow of a viscous electrically conducting incompressible non Newtonian fluid flow taking place in a horizontally placed channel composed of upper impermeable wall and naturally permeable bottom. The flow is driven by the shear generated due to the motion of the upper wall having velocity U_0 in its plane. The porous base is assumed to enable hydrodynamic slip. A Cartesian coordinate system is chosen as shown in the Figure-1. A uniform magnetic field B_0 is applied along the normal direction of the flow. Since the flow is hydrodynamically and thermally fully developed, hence the fluid velocity u and the fluid temperature T depend on y only. Hence, the setup described above is given as follows [Vyas and Yadav[27]]

$$\mu\frac{d^2u}{dy^2} + 6\beta\left(\frac{du}{dy}\right)^2\frac{d^2u}{dy^2} - \sigma {B_0}^2 u = 0 \ldots (1) \quad (1)$$

$$\kappa\frac{d^2T}{dy^2} + \delta\left(\frac{du}{dy}\right)^2\left[\mu + 2\beta\left(\frac{du}{dy}\right)^2\right] + \sigma B_0^2 u^2 = 0 \ldots (2) \quad (2)$$

The end constraints are

$$y = 0; u = \frac{\sqrt{K_0}}{\alpha}\frac{du}{dy}, T = T_1 \ldots (3) \quad (3)$$

$$y = H; u = U_0, T = T_2 \ldots (4) \quad (4)$$

The hydrodynamic slip at y=0 is in accordance with Saffman [21]. Further, the quantities u, μ, σ , κ, β, K_0, H, B_0 , U_0, T_1 and T_2 denote fluid velocity, coefficient of viscosity, electric conductivity, thermal conductivity, non-Newtonian parameter, permeability, height of the channel, applied magnetic field, velocity of upper wall, temperatures of lower and upper wall respectively.

We define

$$K = \frac{K_0}{H^2}, \eta = \frac{y}{H}, u^* = \frac{u}{U_0}, \theta = \frac{T - T_1}{T_2 - T_1} \ldots (5) \quad (5)$$

On using (5), the equations (1)-(4) become:

$$\frac{d^2u^*}{d\eta^2} + 6N\left(\frac{du^*}{d\eta}\right)^2\frac{d^2u^*}{d\eta^2} - M^2u^* = 0 \ldots (6) \quad (6)$$

$$\frac{d^2\theta}{d\eta^2} + \delta Br\left(\frac{du^*}{d\eta}\right)^2\left[1 + 2N\left(\frac{du^*}{d\eta}\right)^2\right] + M^2Bru^{*2} = 0 \ldots (7) \quad (7)$$

$$\eta = 0; u^* = \frac{\sqrt{K}}{\alpha}\frac{du^*}{d\eta}, \theta = 0 \ldots (8) \quad (8)$$

$$\eta = 1; u^* = 1, \theta = 1 \ldots (9) \quad (9)$$

Where

$$M^2 = \frac{\sigma B_0^2 H^2}{\mu}, \qquad N = \frac{\beta U_0^2}{\mu H^2}, \qquad Br = \frac{\mu U_0^2}{\kappa(T_2 - T_1)}$$

Stand for square of Hartmann number, non-Newtonian parameter and Brinkman number respectively

Skin friction and Nusselt number

We intend to compute local skin friction coefficient C_{f_x}, and the local Nusselt number N_{u_x} defined as follows

$$C_{fx} = \frac{\tau_w}{\frac{1}{2}\rho U_0^2}, N_{u_x} = \frac{x q_w}{\kappa(T_2 - T_1)}$$

Where shear stress τ_w, and heat flux q_w are

$$\tau_w = \mu\frac{\partial u}{\partial y} + 2\beta\left(\frac{\partial u}{\partial y}\right)^3 \text{ and } q_w = -\kappa\left(\frac{dT}{dy}\right).$$

to yield,

$$\frac{1}{2}ReC_{fx} = \frac{du^*}{d\eta} + 2N\left(\frac{du^*}{d\eta}\right)^3 \text{ and } \frac{N_{u_x}}{A} = -\frac{d\theta}{d\eta}$$

Where $Re = \frac{U_0 H}{\nu}$ (Reynold number) $A = \frac{x}{H}$ (characteristic length)

Solution

The equations (5)-(9) represent the phenomenon under study. The inherent nonlinearity of these equations is a hindrance to straight forward solution. Therefore, a quest for satisfactory solution strategy is desirable. We adopted semi analytical differential transform method that splendidly handles both linear and nonlinear boundary value problems. Furthermore, in order to validate the semi analytical solution, we exploited Runge-Kutta Fehlberg method also to be performed on rkf45 built in Maple 18 routine. Thus robust computations revealed that pertinent quantities computed from both the methods were in good agreement. A brief of the differential transform method for interested readers is as follows. The differential transformation method pins on employing Taylor series expansion that yields analytical solution in a form of polynomial.

The differential transform of the function f(η) is defined as

$$F(k) = \frac{1}{k!}\left[\frac{d^k f(\eta)}{d\eta^k}\right]_{\eta=\eta_0} \ldots \quad (15)$$

The inverse differential transform of F (k) is defined

$$f(\eta) = \sum_{k=0}^{\infty} F(k)(\eta - \eta_0)^k \quad (16)$$

On combining equation (15) and (16), the f(η) is obtained as

$$f(\eta) = \sum_{k=0}^{\infty} \frac{1}{k!}\left[\frac{d^k f(\eta)}{d\eta^k}\right]_{\eta=\eta_0} (\eta - \eta_0)^k \quad (17)$$

To make the problem determinate, the f(η) in (17) is considered as a sum of finite number of terms say N of the series.

Here N is referred to as size of the series, and the residual terms $\sum_{k=N+1}^{\infty} F(k)(\eta-\eta_0)^k$ are practically assumed to be vanishingly small. In the present case, we find that N=20 is good enough choice for accuracy of order10^{-9}.

When $\eta_0 = 0,$ then expression for f(η) is obtained as

$$f(\eta) = \sum_{k=0}^{N} \frac{\eta^k}{k!}\left[\frac{d^k f(\eta)}{d\eta^k}\right]_{\eta=0} \tag{19}$$

The **Differential Transform method** provides solution in power series of η. It differs from the Taylor's series method in the sense that latter needs coefficients of powers of η whereas the former offers an iterative procedure to find the coefficients.

Some basic well known properties for Differential transforms are represented in table-1

Table-1: Differential transforms of a few functions of interest

Original function	Transform Transformed function
$f(\eta) = f_1(\eta) \pm f_2(\eta)$	$f(\eta) = F_1(k) \pm F_2(k)$
$f(\eta) = C_1 f_1(\eta) \pm C_2 f_2(\eta)$	$f(\eta) = C_1 F_1(\boldsymbol{k}) \pm C_2 F_2(\boldsymbol{k})$
$\boldsymbol{f(\eta) = \frac{d^n f_1(\eta)}{d\eta^n}}$	$\mathrm{F(k)} = \frac{(\mathrm{k}+\mathrm{n})!}{k!}\mathrm{F1(k+n)}$
$f(\eta) = f_1(\eta) f_2(\eta)$	$\mathrm{F(k)} = \sum_{r=0}^{k} \mathrm{F1(r)F2(k-r)}$
$\mathrm{f(\eta) = \eta^n}$	$\mathrm{F(k)} = \Delta(\mathrm{k-n}) = \begin{cases} 1 \text{ if } \mathrm{k} = \mathrm{n} \\ 0 \text{ if } \mathrm{k} \neq \mathrm{n} \end{cases}$

The differential transforms of the functions appearing in equations (6)-(7) are taken to yield the following transformed equations of momentum and energy respectively.

$$(m+1)(m+2)F(m+2) + 6N\left[\sum_{k=0}^{m}\left(\sum_{j=0}^{k}(j+1)F(j+1)(k-j+1)F(k-j+1) = 0\right)(m-k+1)(m-k+2)F(m-k+2)\right] - M^2F(m) \ldots (20) \tag{20}$$

and

$$(m+1)(m+2)T(m+2) + \delta Br\left[\sum_{k=0}^{m}(k+1)F(k+1)(m-k+1)F(m-k+1) + 2N\left(\sum_{k=0}^{m}\left(\sum_{j=0}^{k}\left(\sum_{i=0}^{j}(i+1)F(i+1)(j-i+1)F(j-i+1)\right)(k-j+1)F(k-j+1)\right)(m-k+1)F(m-k+1)\right)\right] + M^2Br\sum_{k=0}^{m}F(k)F(m-k) = 0 \ldots (21) \quad (21)$$

The transformed end conditions are:

$$F[1] = a_1 ; F[0] = \frac{\sqrt{K}}{\alpha}a_1$$

$$T[0] = 0; T[1] = a_2 \quad (22)$$

Where F[k] and T[k] represent differential transform of the functions f(η) and θ(η) respectively and a_1, a_2 are the constants to be determined. The equations (20)-(22) provide F(k) and T(k). We find expressions of F(k) and T(k) for some K as follows

$$F[2] = \frac{1}{2}\frac{M^2\sqrt{K}a_1}{\alpha(6Na_1^2+1)}$$

$$F[3] = -\frac{1}{6}\frac{M^2a_1(-36N^2a_1^4\alpha^2 + 12KM^2Na_1^2 - 12Na_1^2\alpha^2 - \alpha^2)}{\alpha^2(6Na_1^2+1)^3}$$

$$F[4] = \frac{1}{24}\frac{1}{\alpha^3(6Na_1^2+1)^5}\left(M^4\sqrt{K}a_1(-1080N^3a_1^6\alpha^2 + 360KM^2N^2a_1^4 - 324N^2a_1^4\alpha^2 - 12KM^2Na_1^2 - 18Na_1^2\alpha^2 + \alpha^2)\right) \ldots . (23)$$

$$T[2] = -\frac{1}{2}\frac{Bra_1^2(2Na_1^2\alpha^2\delta + KM^2 + \alpha^2\delta)}{\alpha^2}$$

$$T[3] = -\frac{1}{3}\frac{M^2Br\sqrt{K}a_1^2(4Na_1^2\delta + 6Na_1^2 + \delta + 1)}{\alpha(6Na_1^2+1)}$$

$$T[4] = -\frac{1}{12}\frac{1}{\alpha^2(6Na_1^2+1)^3}\big(Bra_1^2M^2(144N^3a_1^6\alpha^2\delta + 216N^3a_1^6\alpha^2 + 24KM^2N^2a_1^4\delta + 36KM^2N^2a_1^4 + 84N^2a_1^4\alpha^2\delta + 108N^2a_1^4\alpha^2 + 6KM^2Na_1^2\delta + 12KM^2Na_1^2 + 16Na_1{}^2\alpha^2\delta + 18Na_1^2\alpha^2 + KM^2\delta + KM^2 + \alpha^2\delta + \alpha^2)\big) \ldots (24) \quad (24)$$

The original functions f(η) and θ(η) are obtained on performing inverse transformation of (23)-(24). Then, on applying the boundary conditions (9), the constants a_1, a_2 are found. Consequently, we find

$$f(\eta) = \frac{\sqrt{K}}{\alpha}a_1 + a_1\eta + \frac{1}{2}\frac{M^2\sqrt{K}a_1}{\alpha(6Na_1^2+1)}\eta^2 - \frac{1}{6}\frac{M^2a_1(-36N^2a_1^4\alpha^2 + 12KM^2Na_1^2 - 12Na_1^2\alpha^2 - \alpha^2)}{\alpha^2(6Na_1^2+1)^3}\eta^3 + \frac{1}{24}\frac{1}{\alpha^3(6Na_1^2+1)^5}\Big(M^4\sqrt{K}a_1(-1080N^3a_1^6\alpha^2 + 360KM^2N^2a_1^4 - 324N^2a_1^4\alpha^2 - 12KM^2Na_1^2 - 18Na_1^2\alpha^2 + \alpha^2)\Big)\eta^4 \ldots . (25) \quad (25)$$

$$\theta(\eta) = a_2\eta - \frac{1}{2}\frac{Bra_1^2(2Na_1^2\alpha^2\delta + KM^2 + \alpha^2\delta)}{\alpha^2}\eta^2 - \frac{1}{3}\frac{M^2Br\sqrt{K}a_1^2(4Na_1^2\delta + 6Na_1^2 + \delta + 1)}{\alpha(6Na_1^2+1)}\eta^3 - \frac{1}{12}\frac{1}{\alpha^2(6Na_1^2+1)^3}\big(Bra_1^2M^2(144N^3a_1^6\alpha^2\delta + 216N^3a_1^6\alpha^2 + 24KM^2N^2a_1^4\delta + 36KM^2N^2a_1^4 + 84N^2a_1^4\alpha^2\delta + 108N^2a_1^4\alpha^2 + 6KM^2Na_1^2\delta + 12KM^2Na_1^2 + 16Na_1{}^2\alpha^2\delta + 18Na_1^2\alpha^2 + KM^2\delta + KM^2 + \alpha^2\delta + \alpha^2)\big)\eta^4 \quad \ldots (26) \quad (26)$$

The equations (25) and (26) present velocity and temperature as a convergent series in terms of η and parameters. For select values of these, we finally get f(η) and θ(η) as a power series in η. For example, when the $M = 1, \alpha = 1, \delta = 1, N = 5, Br = 2, K = 0.1$, then f(η) = .2370487297 + .7496139022η + 0.6637183342e-2η2 + 0.6922237953e-2η3- 0.1429295762e-3η4 …. and θ(η) = 5.137341472η - 3.775665232η^2 - .1996501703η3- .1587027008η4…… After having f(η) and θ(η), we compute f'(η) and θ'(η) too as we require these quantities in entropy computation to be taken in next section.

Thermodynamic Irreversibility

The volumetric rate of entropy S_G for the model is given as (Vyas et al.[24] Vyas and Ranjan [32])

$$S_G = \frac{\kappa}{T_1^2}\left(\frac{\partial T}{\partial y}\right)^2 + \frac{1}{T_1}\left[\delta\left(\frac{du}{dy}\right)^2\left\{\mu + 2\beta\left(\frac{du}{dy}\right)^2\right\}\right] + \frac{\sigma B_0^2u^2}{T_1} \quad (27)$$

we prescribe the following characteristic quantities viz. characteristic entropy and characteristic temperature ratio,

$$S_{G_0} = \frac{\kappa(T_2 - T_1)^2}{T_1^2 H^2}$$

$$\omega = \frac{T_1}{T_2 - T_1}$$

Finally we have entropy number N_s and Bejan number Be as follows

$$N_s = \frac{S_G}{S_{G_0}} = \left(\frac{d\theta}{d\eta}\right)^2 + Br\omega\left[\delta\left(\frac{du^*}{d\eta}\right)^2\left\{1 + 2N\left(\frac{du^*}{d\eta}\right)^2\right\} + M^2u^{*2}\right] \quad (28)$$

$$\text{Be} = \frac{\left(\frac{d\theta}{d\eta}\right)^2}{\left(\frac{d\theta}{d\eta}\right)^2 + Br\omega\left[\delta\left(\frac{du^*}{d\eta}\right)^2\left\{1+2N\left(\frac{du^*}{d\eta}\right)^2\right\}+M^2u^{*2}\right]} \quad (29)$$

Validation

The differential transform method was invoked to simulate the mathematical model under study. We also applied RungeKutta Fehlberg method to the model to ensure the validation with prescribed error tolerance of order 10^{-9} magnitude. The validation is manifested by the quantities computed by both the methods as showcased in Table-2 and Table-3. The table-2 presents values of f (η) and θ(η) computed by DTM and numerically at spatial distance η at intervals of 0.1. We observe that both f (η) and θ(η) do match excellently. Furthermore, the Table-3 reveals that values of skin friction and Nusselt number also do match excellently. Thus, we conclude that solution strategy of both methods validate each other.

Table-2: When $M = 1, \alpha = 1, \delta = 1, N = 5, Br = 2, K = 0.1$

η	$f(\eta)$		$\theta(\eta)$	
	Semi analytical solution by DTM	Numerical solution by RKF45	Semi analytical solution by DTM	Numerical solution by RKF45
0	0.2370487297	0.2370487296	0	0
0.1	0.3120833987	0.3120833987	0.4757619513	0.4757619513
0.2	0.3872921193	0.3872921192	0.8745897834	0.8745897839
0.3	0.4627157837	0.4627157834	1.194710358	1.194710358
0.4	0.5383947432	0.5383947431	1.433962606	1.433962605
0.5	0.6143687191	0.6143687191	1.589792860	1.589792860
0.6	0.6906767175	0.6906767174	1.659249391	1.659249391
0.7	0.7673569533	0.7673569532	1.638976158	1.638976157
0.8	0.8444467827	0.8444467826	1.525205780	1.525205779
0.9	0.9219826429	0.9219826427	1.313751767	1.313751767
1.0	0.9999999999	1.000000000	0.9999999998	1.000000000

Table-3: Skin friction and Nusselt Number (when $\delta = 1$)

M	α	N	Br	K	$\frac{1}{2} Re\, C_{f_x}$ at $y = 0$		$\frac{1}{A} N_{u_x}$ at $y = 0$		$\frac{1}{2} Re\, C_{f_x}$ at $y = 1$		$\frac{1}{A} N_{u_x}$ at $y = 1$	
					DTM	NUM	DTM	NUM	DTM	NUM	DTM	NUM
1	1	5	2	0.2	3.809617124	3.809617127	-4.046813144	-4.046813147	4.457989641	4.457989642	2.555490288	2.555490291
1	1	5	2	0.3	3.166652612	3.166652614	-3.491597083	-3.491597085	3.835931956	3.835931957	1.985178708	1.985178711
1	1	5	2	0.5	2.426920183	2.426920182	-2.909420543	-2.909420542	3.123667582	3.123667583	1.379977568	1.379977566
1	1	5	2	0.1	1.597447990	1.597447989	-2.345739341	-2.345739340	2.331474264	2.331474263	0.779016363	0.779016362
1	1	5	2	0.3	3.166652612	3.166652614	-3.491597083	-3.491597085	3.835931956	3.835931957	1.985178708	1.985178711
1.5	1	5	2	0.3	2.964176326	2.964176328	-3.892293879	-3.892293881	4.449808232	4.449808236	3.004304455	3.004304457
2	1	5	2	0.3	2.710077438	2.710077465	-4.42967426	-4.429674298	5.304492643	5.304491338	4.410705524	4.410705553
2.5	1	5	2	0.3	2.425253353	2.425255147	-5.083714784	-5.083717691	6.393448257	6.393344007	6.187805123	6.187810403
1	2	5	2	0.1	7.120741802	7.12074180	-7.44874587	-7.44874586	7.686383882	7.68638388	5.997234390	5.997234399
1	3	5	2	0.1	8.130591317	8.13059131	-8.630088665	-8.630088657	8.676130472	8.676130467	7.183536121	7.18353611
1	4	5	2	0.1	8.710674408	8.71067441	-9.334059863	-9.334059877	9.245388186	9.245388199	7.889422244	7.889422266
1	5	5	2	0.1	9.086406329	9.08640632	-9.799366462	-9.799366462	9.614355603	9.614355592	8.355657604	8.355657600
2	0.5	5	2	0.3	1.102678382	1.10147747	-3.52927273	-3.52674296	3.780606375	3.909158263	3.305131967	3.301250101
2	0.5	10	2	0.3	2.122656023	2.122656022	-4.153711192	-4.153711191	5.027354728	5.027354809	3.862552674	3.862552671
2	0.5	15	2	0.3	3.177977680	3.177977680	-4.716725141	-4.716725140	6.122969517	6.122969521	4.398135632	4.398135637
2	0.5	20	2	0.3	4.246263415	4.246263415	-5.259667235	-5.259667235	7.213508235	7.213508228	4.926029464	4.926029465
1	1	5	2	0.1	4.961851855	4.961851854	-5.137341472	-5.137341472	5.577608509	5.577608506	3.665474188	3.665474183
1	1	5	3	0.1	4.961851855	4.961851854	-7.206012208	-7.206012208	5.577608509	5.577608506	5.998211285	5.998211275
1	1	5	4	0.1	4.961851855	4.961851854	-9.274682945	-9.274682944	5.577608509	5.577608506	8.330948375	8.330948367
1	1	5	5	0.1	4.961851855	4.961851854	-11.34335368	-11.34335368	5.577608509	5.577608506	10.66368548	10.66368545

2. Results and Discussion

The skin friction and Nusselt number are pertinent quantities as they offer the rate of shear and rate of heat transfer which is useful to design optimal system. We note that when M=1=α=δ, N=5, Br=2 and the permeability K of porous lining is increased from K=0.2 to 1 then there is a decrease in coefficient of skin friction at the lower wall from a value 3.809617124 to 1.597447990 and the skin friction at the upper wall reduces from a value 4.457989641 to 2.331474264. Similarly, the Nusselt number at the lower wall increases from a value -4.046813144 to -2.345739341 and the Nusselt number at the upper wall reduces from 2.555490291 to 0.779016362. It is important revelation to note that permeability of a permeable strata allowing hydrodynamic slip may prove to be a pertinent instrument in flow and heat transfer management mechanism.

When K=0.3, α=1=δ, N=5, Br=2 and the Hartmann number is raised from a value M=1 to 2.5 then the skin friction coefficient at the lower wall is decreased from a value 3.166652612 to 2.425253353 and it swell up from a value 3.835931956 to 6.393448257 at the upper wall. For the same set of values, the Nusselt number at the lower wall decays from a value -3.491597083 to -5.083714784 whereas it augments from 1.985178708 to 6.187805123 at the upper wall. When M=1=δ, N=5, Br=2, K=0.1 and the α is raised from 2 to 5, then the skin friction coefficient is increased from a value 7.120741802 to 9.086406329 at the lower wall and it increases from a value 7.686383882 to 9.614355603 at the upper wall. For the same variation, the Nusselt number at the lower wall changes from a value -7.44874587 to -9.799366462 and the Nusselt number at the upper wall changes from 5.997234399 to 8.355657600.

When the parameters are kept fixed as M=2, α=0.5, δ=1, K=0.3, Br=2 and the value of N is raised from 5 to 20 then the coefficient of skin friction at the lower wall is increased from a value 1.102678382 to 4.246263415 and the skin friction at the upper wall changes from a value 3.780606375 to 7.213508235. Nusselt number at the lower wall for the same variation changes from a value -3.52927273 to -5.259667235 and the Nusselt number at the upper wall changes from 3.305131967 to 4.926029464.

When the other parameters are kept fixed as M=1=α=δ, N=5, K=0.1 and the Brinkman number is raised from a value Br=2 to 5 then the coefficient of skin friction remains unchanged at the both wall whilst for the same variation, the Nusselt number changes from a value -5.137341472 to -11.34335368 at the lower wall and from a value 3.665474188 to 10.66368548 at the upper wall. In order to see the entropy distribution, we needed velocity and temperature regimes and respective gradients as evinced from equation (27). The figures 2-5 and 6-10 portray the distribution of these quantities as a ready reference to peep into the phenomenon as we are not presenting a discussion on them.

Before we make detailed discussion on plots of irreversibility, we are inclined to offer a few remarks. The entropy quantified as number Ns entails key information about dependence of thermodynamic irreversibility on the embedded parameters. It creates the basis for the desired understanding of involved intricacies. In fact a plot of Ns reveals key information. Further, Bejan number is to offer picture of relative importance of irreversibility caused by heat transfer to total irreversibility.

The figure11 presents entropy for the variation of slip coefficient α. It is observed that with an increase in α, there is a rise in entropy. We recall experimentation by Beavers and Joseph (1967) that revealed that slip coefficient α depends on non-uniformities in the arrangement of porous matrix at the clear-porous surface, the flow direction at the interface, the extent of the clear fluid, and the Reynold's number. They computed values for slip coefficient α for different materials e.g. α =0.1 for aloxite with average pore size 0.027 inches and slip coefficient α takes values 1.45 and 4.0 for foametal with average pore sizes 0.034 and 0.045 inches. It is not out of place to reiterate that as the slip coefficient α depends very much on non-uniformities in the arrangements of particles in the porous matrix and porous media having same permeability or same bulk porosity may

come up with distinct values of α. Therefore, the slip coefficient α sounds to be a pertinent entropy management parameter without having a bearing on the permeability.

The figure 12 shows variation in Ns for varying Br when the parameters M, α, δ N, K are fixed. We note that rising Br i.e. rising dissipation enhances entropy. It goes well with the physical understanding that energy loss due to dissipation is not reversible process. The figure 13 shows variation of Ns for varying K when M, α, δ, N and Br are kept fixed. It is noted that entropy declines with a rise in permeability. Thus permeability of the porous base affects the flow and heat in the system. The effect is of immense significance that suggests inclusion of finer porous strip as an effective thermodynamic irreversibility management tool. The figure 14 shows variation of Ns for varying Hartmann number M to reveal that entropy rises with augmenting Hartmann number. In fact, higher values of M retards the flow and cause sharp temperature gradients which lead to larger entropy. The figure 15 shows variation in Ns for varying non Newtonian parameter N. The figure reveals that when the fluid deviates from Newtonian character then entropy is bound to rise. The figures 16-20 portray Bejan number distribution across the channel. Here it is seen that Be vanishes at different spatial distances in the channel for chosen values of parameters. Before analysing the Be plots we make certain remarks about Bejan number. The point where Be=0 refers to the case when there is no heat transfer irreversibility and Be=1 refers to the situation when there is no irreversibility due to dissipations. With this understanding one may peep into relative importance of irreversibility due to heat transfer and dissipations for designated parameters' effects.

3. Conclusions

The study revealed a successful execution of DTM and R-K-Fehlberg 45 numerical strategy to the model under consideration. It offered important data set for skin friction, Nusselt number to validate future studies. Worth mentioning points are follows

1. The coefficient of skin friction at the walls is seen decreased with an increase in Darcy number K. The Nusselt number at the lower wall numerically increases with an increase in Darcy number K. However, the Nusselt number at the upper wall decreases with an increase in Darcy number K.
2. When the Hartmann number is raised then there is a decay in skin friction at the lower wall whereas an increase in skin friction at the upper wall is noted. For the same values of parameters, the Nusselt number at the lower wall decreases and the Nusselt number at the upper wall increases.
3. When the slip parameter α is raised then the there is rise in skin friction at the both the walls. For the same values of parameters, the Nusselt number at the lower wall in noted decreased and the Nusselt number at the upper wall is found increased.
4. When the value of N is raised then then the there is rise in skin friction at the both the walls. For the same values of parameters, the Nusselt number at the lower wall in noted decreased and the Nusselt number at the upper wall is found increased.

5. When the Brinkman number is raised then the coefficient of skin friction remains unchanged at the both wall whilst for the same values of parameters, the Nusselt number at the lower wall in noted decreased and the Nusselt number at the upper wall is found increased.

6. The entropy shows qualitative and quantitative sensitivity towards embedded parameters.

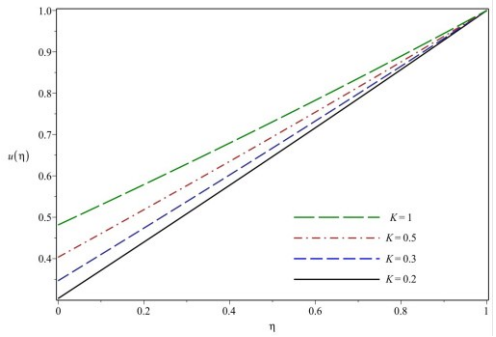

Fig. 2 variation in u when M=1, α=1, δ=1, N=5, Br=2,

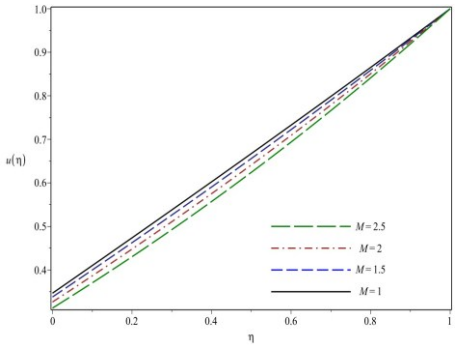

Fig. 3 variation of u when α=1, δ=1, N=5, Br=2, K=0.3

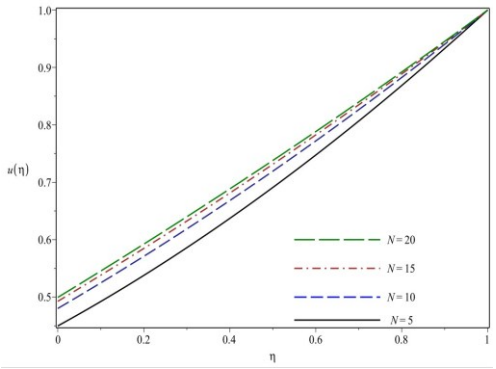

Fig. 4 profiles of u when M=2, α=0.5, δ=1, Br=2, K=0.3

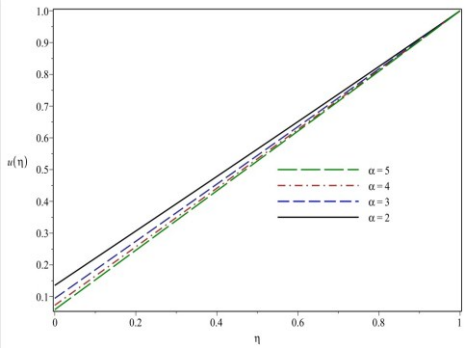

Fig. 5 profiles of u when M=2, N=5, δ=1, Br=2, K=0.3

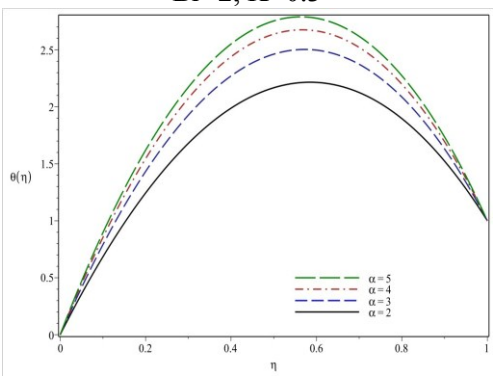

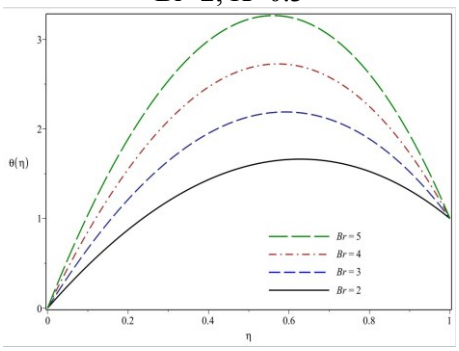

Fig. 6 profiles of θ when M=1, δ=1, N=5, Br=2, K=0.1

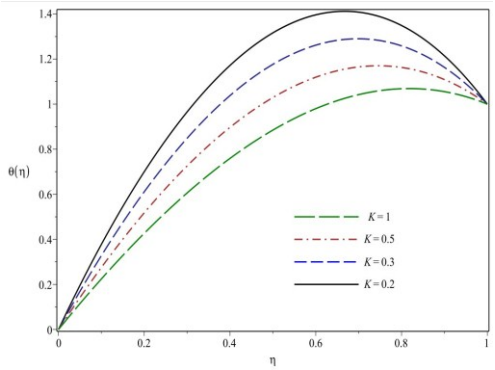

Fig. 7 profiles of θ when M=1, α=1, δ=1, N=5, K=0.1

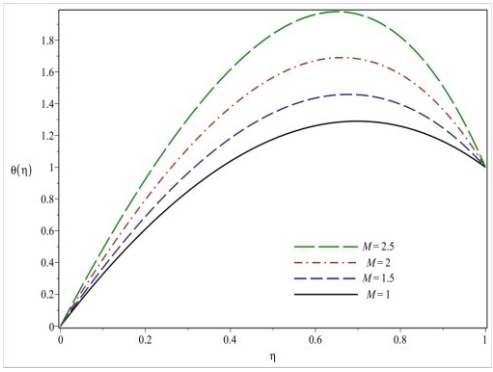

Fig.8 profiles of θ when M=1, α=1, δ=1, N=5, Br=2

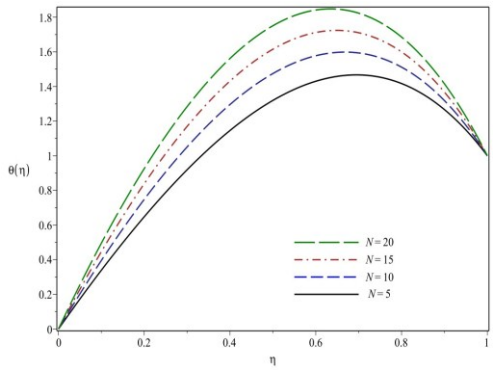

Fig. 9 profiles of θ when α=1, N=5, δ=1, Br=2, K=0.3

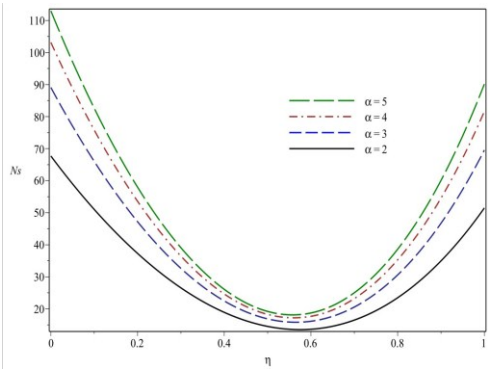

Fig. 10 profiles of θ when M=2, α=0.5, δ=1, Br=2, K=0.3

Fig. 11 profiles of Ns when M=1, δ=1, N=5, Br=2, K=0.1

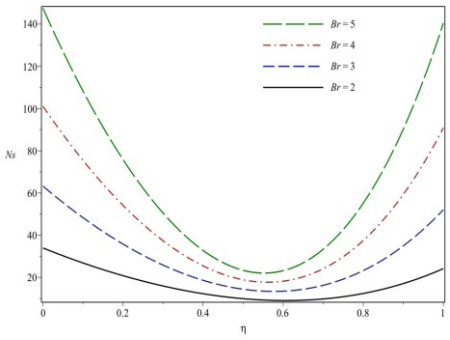

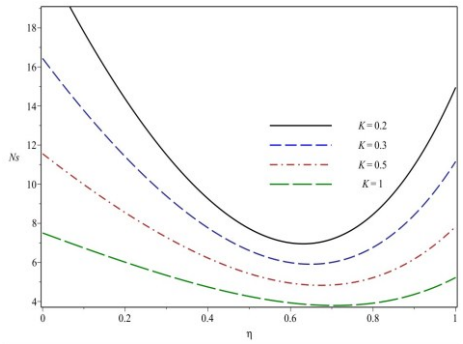

Fig. 12 profiles of Ns when M=1, α=1, δ=1, N=5, K=2

Fig. 13 profiles of Ns when M=1, α=1, δ=1, N=5, Br=2

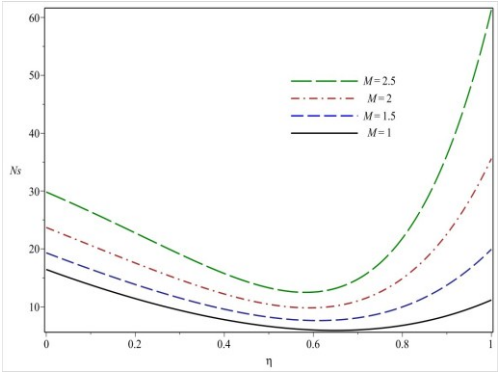

Fig. 14 profiles of Ns when α=1, δ=1, N=5, Br=2, K=0.3

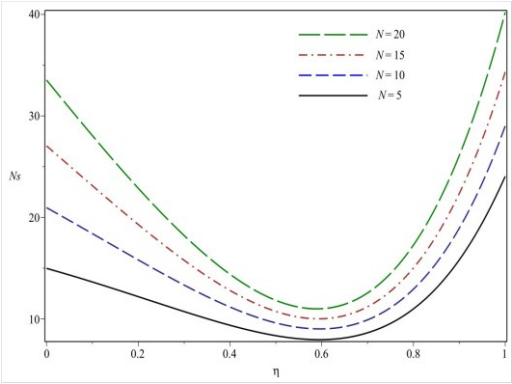

Fig. 15 profiles of Ns when M=2, α=0.5, δ=1, Br=2, K=0.3

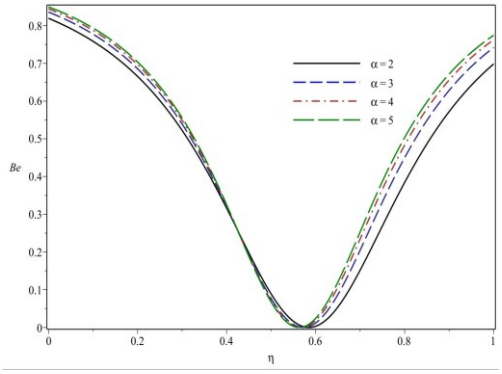

Fig. 16 profiles of Be when M=1, δ=1, N=5, Br=2, K=0.1

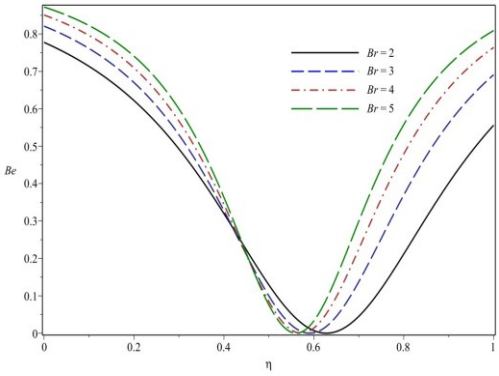

Fig. 17 profiles of Be when M=1, α=1, δ=1, N=5, K=0.1

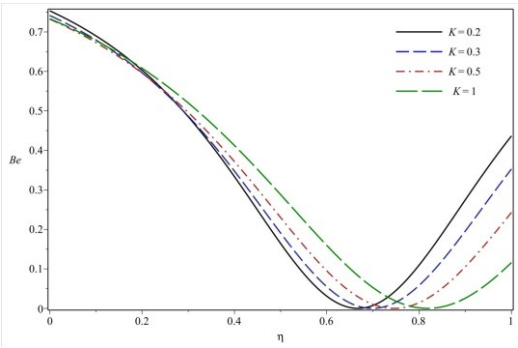

Fig. 18 profiles of Be when M=1, α=1, δ=1, N=5, Br=2

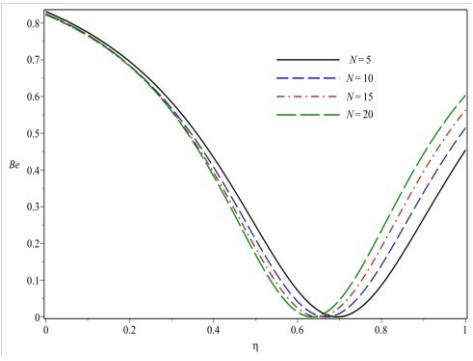

Fig. 19 profiles of Be when M=2, α=0.5, δ=1, Br=2,K=0.3

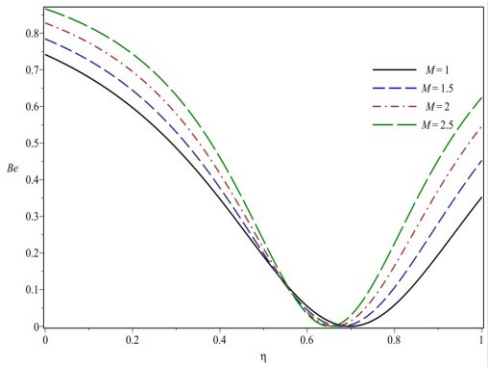

Fig. 20 profiles of Be when α=1, δ=1, N=5, Br=2, K=0.3

References

[1] Alves, M. A., Pinho, F. T. and Oliveira, P. J. (2001). Study of steady pipe and channel flows of a single-mode Phan-Thien-Tanner fluid, *Journal of Non-Newtonian Fluid Mechanics*. **101**(1–3), 55-76.

[2] Azaiez,J., Guénette, R. and Aït-Kadi, A. (1996). Numerical simulation of viscoelastic flows through a planar contraction, *Journal of Non-Newtonian Fluid Mechanics*. **62**(2–3), 253-277.

[3] Bataineh, A. S. Isik, O.R. Hashim, I. (2016). Bernstein method for the MHD flow and heat transfer of a second grade fluid in a channel with porous wall, *Alexandria Engineering Journal*, **55**, 2149-2156.

[4] Bejan, A. (1982). Second-law analysis in heat transfer and thermal design, *Adv. Heat Transfer*. **15**, 1-58.

[5] Bejan, A. (1979). A study of entropy generation in fundamental convective heat transfer, *J. Heat Transf*. **101**, 718-725.

[6] Bejan, A. (1996), *Entropy Generation Minimization*, CRC press.

[7] Chen, Y. and Zhu, K. (2008). Couette-poisieille flow of Bingham fluids between two porous parallel plates with slip conditions, *J. Non-Newtonian Fluid Mech*. **153**, 1-11.

[8] Devakar, M., Ramesh, K., Chouhan, S. Raje, A. (2017). Fully developed flow of non-Newtonian fluids in a straight uniform square duct through porous medium, *Journal of the Association of Arab Universities for Basic and Applied Sciences*. **23**, 66-74.

[9] Ferrás L, Nébrega J, Pinho F. (2012). Analytical solutions for Newtonian and inelastic non-Newtonian flows with wall slip, *J Non-Newtonian Fluid Mechan*. **175**, 76-88.

[10] Griffiths, P. (2020). Non-Newtonian channel flow—exact solutions, *IMA Journal of Applied Mathematic*. **85**(2), 263-279.

[11] Hosseini, M., Sheikholeslami, Z. and Ganjic, D.D. (2013). Non-Newtonian fluid flow inanaxisymmetric channel with porous wall, P*ropulsion and Power Research*. **2**(4), 254-262.

[12] Ibanez, G., Lopez, A., Pantoja, J., Moreira, J. (2014). Combined effects of uniform heat flux boundary conditions and hydrodynamic slip on entropy generation in a microchannel, *Int. J. Heat Mass Transfer*. **73**, 201-206.

[13] Ibanez, G., Lopez, A., Pantoja, J., Moreira, J., Reyes, J.A. (2013). Optimum slip flow based on the minimization of entropy generation in parallel plate microchannels, *Energy*. **50**, 143-149.

[14] Lopez de haro, M., Cuevas, S., Beltran, A. (2014). Heat transfer and entropy generation in the parallel plate flow of a power-law fluid with asymmetric convective cooling, *Energy*. **66**, 750-756.

[15] Mahmud, S. and Freser, R.A. (2002). Inherent irreversibility of channel and pipe blows for Non-Newtonian fluids, *Int. Commn. Heat Mass Transfer*. **29**, 577-587.

[16] Mitsoulis, E. and Hatzikiriakos, G.S. (2009). Steady flow simulations of compressible PTFE paste extrusion under severe wall slip, *Journal of Non-Newtonian Fluid Mechanics*. **157** (1–2), 26-33.

[17] Oliveira, P. J. and Pinho, F. T. (1999). Analytical solution for fully developed channel and pipe flow of Phan-Thien–Tanner fluids, *Journal of Fluid Mechanics*. **387**, 271-280.

[18] Raisi, A., Mirzazadeh, M., Dehnavi, A.S. and Rashidi, F. (2007). An approximate solution for the Couette–Poiseuille flow of the Giesekus model between parallel plates, *Rheologica Acta*. **47**, 75-80.

[19] Ravanchi, M.T., Mirzazadeh, M. and Rashidi, F. (2007). Flow of Giesekus viscoelastic fluid in a concentric annulus with inner cylinder rotation, International Journal of Heat and Fluid Flow. **28**(4), 838-845.

[20] Rosales, I.G., Duharte, G.I., López Grijalva, A., LastresDanguillecourt, O., Reyes- Nava, J.(2020). Entropy generation minimization and nonlinear heat transport in MHD flow of a couple stress nanofluid through an inclined permeable channel with a porous medium, *thermal radiation and slip. Heat Transfer*, **49**, 4878-4906.

[21] Saffman, P.G. (1971). On the boundary condition at the surface of a porous medium. *Stud. Appl. Math*. **50**, 93-101.

[22] Schleiniger, G. and Weinacht, R.J. (1991). Steady Poiseuille flows for a Giesekus fluid, *Journal of Non-Newtonian Fluid Mechanics*. **40**(1), 79-102.

[23] Vyas P. and Yadav K. (2020). EGA for a Convective Regime Over a Vertical Cylinder Stretching Linearly, *Applied Mathematics and Nonlinear Sciences*. 1-12.

[24] Vyas P., Khan, S. and G. (2021). Micropolar couple stress thermofludics and entropy in Forchheimer channel, *Heat Transfer*. 1-35.

[25] Vyas, P. and Khan, S. (2016). Entropy analysis for MHD dissipative Casson fluid flow in porous medium due to stretching cylinder, *Acta Technica*. **61**(3), 299-315.

[26] Vyas, P. and Srivastava, N. (2015). Entropy analysis of generalized MHD Couette flow inside a composite duct with asymmetric convective cooling, *Arab. J. Sci. Eng*. **40**, 603-614.

[27] Vyas, P. and Yadav, K. (2021). On entropy generation due to transient MHD radiative free convection with induced magnetic field in a porous medium channel, **50**(8), 7521-7552.

[28] Vyas, P., Gajanand, Khan, S. Irreversibility analysis for Casson thermo-fluidics inside a cone: Cattaneo–Christov heat flux.

[29] Vyas, P., Khan, S., Gajanand (2021). Cattaneo–Christov flux and entropy in thermofluidics involving shrinking surface, **50**(6), 6210-6236.

[30] Vyas, P., Kasana, R.K., Khan, S. (2020). Entropy Analysis for boundary layer Micropolar fluid flow. AIMS Mathematics. **5**(3), 2009-2026.

[31] Vyas, P., Soni, S. (2018). Entropy analysis for boundary layer flow due to a point sink at the vertex of the cone. Acta Technica. **63**(2), 143-156.

[32] Vyas, P. and Ranjan, A. (2015). Entropy analysis of radiative MHD forced convection flow with weakly temperature dependent convection coefficient in porous medium channel, Acta Technica, **60**(1), 1-14.

[33] Vyas, P. and Srivastava, N. (2015). Entropy analysis of generalized MHD Couette flow inside a composite duct with asymmetric convective cooling, *Arabian J. for Science and Engineering*. **40**(2), 603-614.

[34] Yilbas, B.S., Yursoy, M., Pakdemerili, M. (2004). Entropy analysis for non-Newtonian fluid flow in annular pipe, constant viscosity case, *Entropy*. **6**(3), 304-315.

[35] Yoo, J.Y. and Choi, H. Ch. (1989). On the steady simple shear flows of the one-mode Giesekus fluid, *Rheologica Acta*. **28**, 13-24.